

A Significant Two-Dimensional Structural Transformation in a Coordination Polymer that Changes Its Electronic and Protonic Behavior

Yao Jing,^[a] Yukihiro Yoshida,^{*[a]} Tokutaro Komatsu,^[b] and Hiroshi Kitagawa^{*[a]}

[a] Y. Jing, Prof. Y. Yoshida, Prof. H. Kitagawa
Division of Chemistry, Graduate School of Science, Kyoto University
Kitashirakawa-Oiwakecho, Sakyo-ku, Kyoto 606-8502 (Japan)
E-mail: yoshiday@ssc.kuchem.kyoto-u.ac.jp, kitagawa@kuchem.kyoto-u.ac.jp

[b] Prof. T. Komatsu
School of Medicine, Nihon University
30-1 Oyaguchi-Kamicho, Itabashi-ku, Tokyo 173-8610 (Japan)

Supporting information for this article is given via a link at the end of the document.

Abstract: A 2D-to-2D (2D: two-dimensional) structural transformation accompanying significant bond rearrangement and coordination environment change is demonstrated in a coordination polymer (CP) comprised of copper(II) ions and terephthalate (BDC²⁻) ligands for the first time. When immersed in water, a free-standing membrane of 2D Cu(BDC)(DMF) (**Cu-1**; DMF: *N,N*-dimethylformamide) transforms into 2D Cu(BDC)(H₂O)₂ (**Cu-2**) while maintaining its highly oriented layered structure. In the 2D sheet, paddlewheel-type Cu(II) dimers coordinated with four bidentate BDC ligands in a square-planar array in **Cu-1** were released to form uniform aqua-bridged Cu(II) chains, which are cross-linked with each other by unidentate BDC ligands, in **Cu-2**. The present facile approach to implement the 2D-to-2D transformation accompanied by bond rearrangement, which is characteristic of CPs, leads to a marked increase in in-plane magnetic susceptibility and proton conductivity. In situ experiments in support of theoretical calculations unveiled the energy diagram that governs the unique structural transformation.

Introduction

Two-dimensional (2D) nanostructured materials have garnered a great deal of attention in diverse research fields, especially after the discovery of graphene in 2004.^[1] This interest is primarily because of their unique chemical and physical properties at the nanoscale, such as their extremely high specific surface area and confined electronic state.^[2] Each 2D assembly in the system constructed by strong covalent bonds is connected to each other by interlayer van der Waals interactions. To date, a variety of approaches have been implemented to control the electronic properties of 2D layered materials; e.g., (1) changing the number of layers to modulate the band structure as found in graphene,^[3] transition metal dichalcogenides (TMDs),^[4] and transition metal carbides (MXenes);^[5] (2) introducing a twist between two layers to induce superconductivity as represented by graphene (so-called “twistronics”);^[6] (3) interpenetrating or interdigitating 2D frameworks in coordination polymers (CPs);^[7] and (4) chemically modifying the surface of materials such as graphene,^[8] TMDs,^[9] and MXenes.^[10] However, it is still challenging to precisely design the atomic or molecular arrangement within a 2D sheet owing to the robust network formed by covalent bonds. To address this challenge, intralayer engineering is a promising approach, as it

leads to the essential modification of chemical and physical properties of the 2D layered materials.

CPs, which are comprised of metal ions or clusters and multidentate organic linkers, have attracted significant attention owing to their high crystallinity and structural tunability.^[11] It is known that judicious selection of the components not only controls the network structure but also introduces functional organic linkers that are responsive to external stimuli.^[2c,12] For example, UV light irradiation induces the [2+2] cycloaddition of photoreactive 1,2-bis(4-pyridyl)ethene linkers in zinc-based 2D CPs while maintaining the coordination environment, leading to a modest change in CO₂ sorption behavior.^[13] We note that the dimensionality of CPs is defined as that of polymeric framework built by covalent or coordination bonds.^[11a] Although a few successful examples of the change in coordination environment (i.e., the change in coordination components) in 2D sheet have been reported,^[2c,12,14] the structural transformation in 2D CPs that accompanies the change in physical properties while maintaining the component ions has never been achieved.

A 2D copper(II) terephthalate CP, Cu(BDC)(DMF) (**Cu-1**), where BDC²⁻ and DMF stand for terephthalate and *N,N*-dimethylformamide, respectively, involves square-grid sheets comprised of copper dinuclear paddlewheel units within the (2 0 -1) plane, where each Cu(II) dimer is coordinated with four BDC ligands in bridging bidentate mode (Figure 1a).^[15] Recently, we have succeeded in realizing reversible multi-dimensional transformations in the CP system while maintaining the component ions,^[16] namely, **Cu-1** to one-dimensional (1D) CP, [Cu(BDC)(H₂O)₂]·H₂O^[17] and **Cu-1** to three-dimensional (3D) CP, Cu(BDC).^[15] During the investigation, we found an unprecedented consecutive transformation; namely, another 2D CP, Cu(BDC)(H₂O)₂ (**Cu-2**),^[17b] was formed as an intermediate phase in the process of the 2D-to-1D transformation in water under stirring at room temperature (RT) (Figure S1). In **Cu-2**, copper ions form a uniform aqua-bridged zig-zag chain along the *c* axis, which is cross-linked to neighboring chains via bridging unidentate BDC ligands to form 2D sheets within the *ac* plane (Figure 1b).^[17b] In this study, we succeeded in stabilizing the metastable **Cu-2** by optimizing the conditions and in achieving an unprecedented 2D-to-2D structural transformation. Of most importance is that the transformation accompanies the significant changes in the bond arrangement and coordination environment

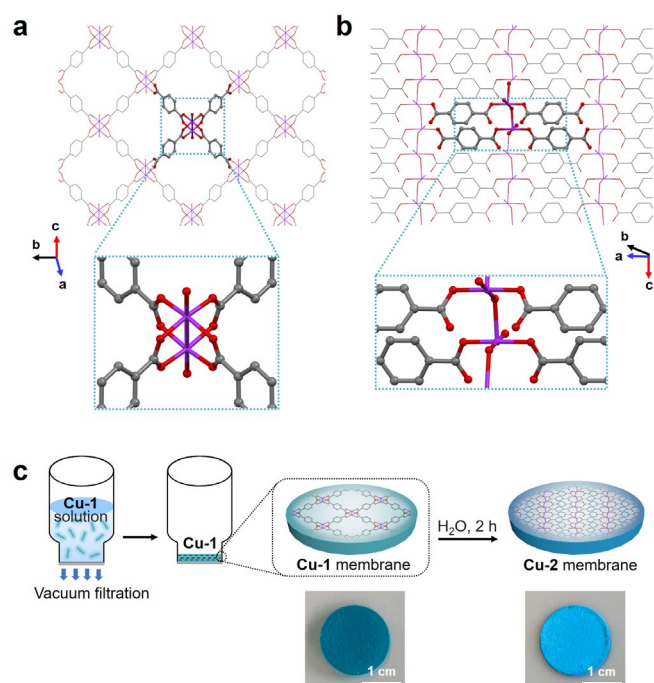


Figure 1. Cu(II) coordination environments in (a) Cu(BDC)(DMF) (**Cu-1**) and (b) Cu(BDC)(H₂O)₂ (**Cu-2**) (gray, C; purple, Cu; red, O). Coordinated solvent molecules are represented as red spheres, and hydrogen atoms are omitted for clarity. The sheet area per BDC ligand is 57.7 Å² in **Cu-1** and 30.7 Å² in **Cu-2**. (c) Schematic illustrations of the fabrication of **Cu-1** membrane followed by transformation into the **Cu-2** membrane, including photos of the **Cu-1** and **Cu-2** membranes.

within the 2D sheets altering their physical properties, in contrast to the aforementioned 2D-to-2D transformations.^{2c,12,14} We found that the structural change greatly affects the in-plane physical properties such as magnetism and proton conduction based on in situ experiments.

Results and Discussion

Blue-green **Cu-1** nanosheets were synthesized through the bottom-up method; namely, the reaction of CuCl₂ with H₂BDC in DMF at RT in the presence of triethylamine as surfactant (see Supporting Information for detailed synthetic procedure).^[18] The powder X-ray diffraction (PXRD) pattern of the as-synthesized **Cu-1** nanosheets is in good agreement with the simulated pattern of the single-crystal XRD data (Figure S2a).^[15a] A more intense peak located at $2\theta = 16.8^\circ$, corresponding to the (2 0 -1) reflection, possibly arises from the preferred orientation of the nanosheets (Figure 2a).^[19] Vacuum filtration of the dispersed DMF solution of **Cu-1** nanosheets yielded the homogeneous membrane on a hydrophobic polytetrafluoroethylene filter (Figure 1c). As expected, the out-of-plane XRD pattern of the membrane displayed intense and well-defined (2 0 -1) and (4 0 -2) reflections (Figure 2c), as a consequence of the highly oriented regular stacking of the **Cu-1** nanosheets in the membrane. The cross-sectional scanning electron microscopy (SEM) image affirmed that the nanosheets were well-oriented in a parallel fashion in the membrane with a thickness of approximately 30 μm (Figure 2e).

Whereas our previous studies suggested that the transformation from **Cu-1** to 1D [Cu(BDC)(H₂O)₂]-H₂O occurs

very fast in water under stirring and thus the intermediate **Cu-2** is quite difficult to isolate,^[16] we found that gentle immersion of the **Cu-1** membrane in water (i.e., without stirring) can stabilize the metastable **Cu-2** phase by virtue of the deceleration of the transformation to 1D [Cu(BDC)(H₂O)₂]-H₂O. It is possible that highly oriented and tightly packed nanosheets, though the in-plane XRD pattern fairly similar to that of PXRD pattern (Figure 2c), as well as the agitation-free conditions suppressed the penetration of water into the membrane to decelerate the transformation sequence. The structural transformation can be clearly discerned by a color change of the membrane from blue-green to sky-blue (Figure 1c). As shown in the out-of-plane XRD patterns (Figure S3), a pronounced peak appeared at $2\theta = 24.5^\circ$ just after immersion of the **Cu-1** membrane for 1 min. Both the in-plane and out-of-plane XRD patterns remained almost unchanged after immersion in water for 2 h. According to the PXRD pattern of the pulverized membrane (Figure S2b), the resulting phase was readily identified as **Cu-2**, where the conversion ratio is nearly equal to unity. The peak at $2\theta = 24.5^\circ$ observed in the out-of-plane XRD pattern (Figure 2d) was assigned to the (0 2 0) reflection of **Cu-2**,^[17b] which indicates that

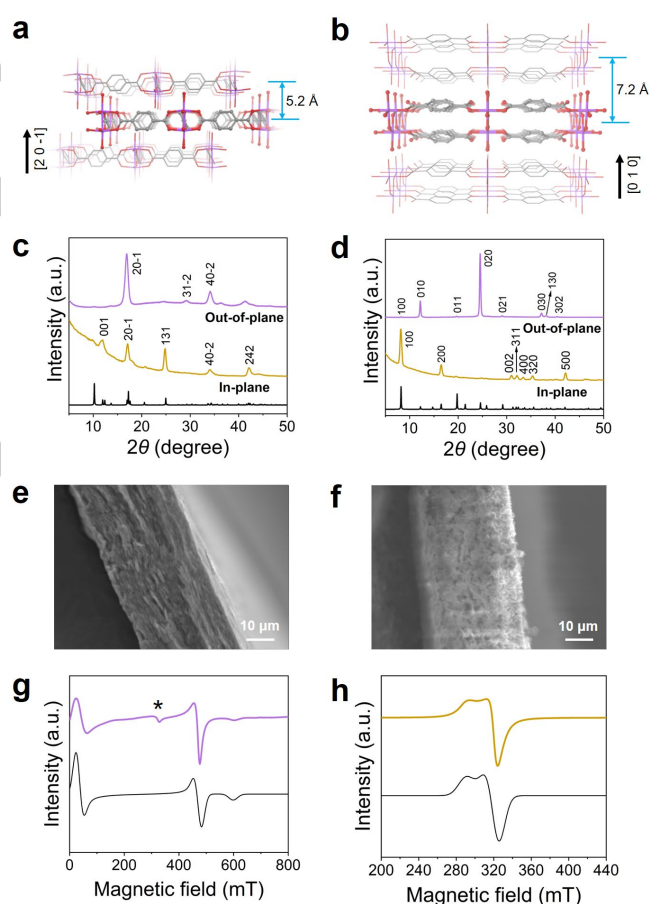


Figure 2. Crystal structures of (a) **Cu-1** and (b) **Cu-2**, where coordinated solvent molecules are represented as red spheres, and hydrogen atoms are omitted for clarity (gray, C; purple, Cu; red, O). The 2D sheets in **Cu-1** and **Cu-2** lie parallel to the (2 0 -1) and (0 1 0) planes, respectively. Out-of-plane (purple), in-plane (orange), and simulated (black) X-ray diffraction (XRD) patterns of (c) **Cu-1** and (d) **Cu-2** membranes. Cross-sectional scanning electron microscopy (SEM) images of (e) **Cu-1** and (f) **Cu-2** membranes. X-band electron spin resonance (ESR) spectra of pulverized (g) **Cu-1** and (h) **Cu-2** membranes at room temperature, where an asterisk indicates the monomeric impurity. Simulated patterns are shown in black.

RESEARCH ARTICLE

the 2D sheets preferentially aligned parallel to the plane of the **Cu-2** membrane. Therefore, it is evident that the orientation of the 2D sheets remains unchanged before (**Cu-1**) and after (**Cu-2**) being immersed in water, while the coordination environment within the sheets undergoes a significant change. The removal of coordinated DMF molecules and subsequent binding of water molecules were confirmed in the infrared (IR) spectra by the disappearance of the O=C–N bending (676 cm^{-1}) and C=O stretching (1663 cm^{-1}) modes of DMF and the appearance of a characteristic broad band corresponding to the O–H stretching mode of water ($2800\text{--}3500\text{ cm}^{-1}$), while maintaining the bands assigned to the benzene ring of BDC²⁻ ligands (1386 , 1154 , and 1018 cm^{-1}) (Figure S5).^[20] The change in coordination environment is also evident from the spectral change in the carboxylate stretching region. The antisymmetric COO⁻ stretching mode in **Cu-1** (1607 cm^{-1}) was red-shifted to 1571 cm^{-1} in **Cu-2**, which is attributed to the change in coordination mode from bridging bidentate (**Cu-1**) to ionic unidentate (**Cu-2**).^[21] Electron spin resonance (ESR) measurements also affirmed the release of dimerized copper units. As shown in Figure 2g, the X-band ESR spectrum of pulverized **Cu-1** membrane exhibits a pattern characteristic of carboxylate-bridged paddlewheel-type Cu(II) dimers with an $S = 1$ spin,^[22] which was well reproduced using anisotropic g factors ($g_x = g_y \equiv g_{\perp} = 2.05$ and $g_z \equiv g_{\parallel} = 2.64$) and zero-field splitting parameter ($D = -0.424\text{ cm}^{-1}$ assuming axial symmetry; i.e., $E = 0$). The sign of D was chosen to be negative according to the ab initio theoretical calculations^[23] and high-frequency ESR measurements.^[24] On the other hand, pulverized **Cu-2** membrane showed two axially symmetric ESR signals ($g_{\perp} = 2.09$ and $g_{\parallel} = 2.32$) characteristic of monomeric Cu(II) ions, where the $g_{\parallel} > g_{\perp}$ trend indicates the occupation of the unpaired electron predominantly on the $d_{x^2-y^2}$ orbital.^[25]

The proposed mechanism of the transformation is shown in Figure S6. The adsorption of water molecules in **Cu-1** induces the cleavage of one of the equatorial Cu–O coordination bonds for each BDC ligand followed by the reorientation of unidentate BDC ligands directed along the c axis (for **Cu-2**; the same hereinafter). Accordingly, the bridging unidentate coordination of BDC along the a axis and water bridging along the c axis (Figure 1b) reconstruct the infinite 2D coordination structure within the ac plane (Figure 2b). The structural transformation entails the elongation of the interplanar distance (5.2 \AA in **Cu-1** and 7.2 \AA in **Cu-2**), whereas the 2D sheet area shrinks owing to the replacement of the BDC ligands with water molecules at the bridging site along the c axis (57.8 \AA^2 in **Cu-1** and 30.7 \AA^2 in **Cu-2** per BDC²⁻). The overturning of nanosheets within the membrane (Figure 2f) possibly arises from the breaking of Cu–O bonds along the c axis and the formation of interlayer O–H \cdots O hydrogen bonds along the b axis (see below). Notably, such a bond reconstruction is manifested in the improved degree of in-plane orientation, as indicated by the in-plane XRD pattern of the **Cu-2** membrane (Figure 2d). The sharp PXRD peaks of pulverized **Cu-2** membrane is compelling evidence of the higher crystallinity upon transformation (Figure S2).

Nanoscale morphologies of the **Cu-1** and **Cu-2** nanosheets in their membranes were examined with transmission electron microscopy (TEM). It is noteworthy that both nanosheets, which were deposited by dropping the suspension after centrifugation and sonication of the membranes immersed in DMF and water, respectively, have a sheet-like structure with a lateral dimension of several micrometers (Figures 3a and 3b). The thickness of the

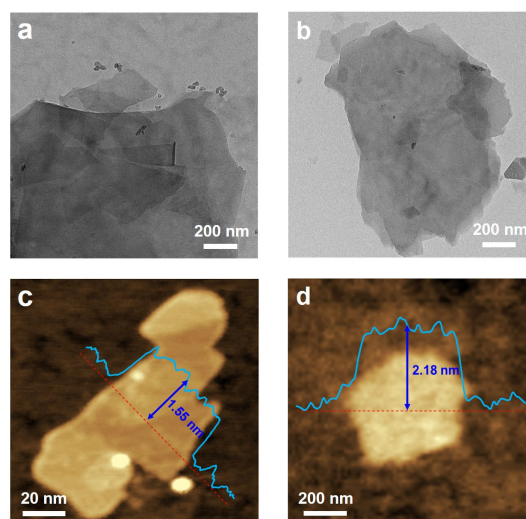


Figure 3. Transmission electron microscopy (TEM) images of (a) **Cu-1** and (b) **Cu-2** nanosheets. Topographies of (c) **Cu-1** and (d) **Cu-2** obtained using atomic force microscopy (AFM), where the pale blue lines show the height profile along the red dotted line in the image.

Cu-1 and **Cu-2** nanosheets was estimated to be 1.55 and 2.18 nm, respectively, using atomic force microscopy (AFM) (Figures 3c, 3d, S7, and S8).

To investigate the effect of the change in the copper coordination environment in the sheets, the magnetic susceptibility of the membrane was measured in situ along the in-plane direction under an ambient helium atmosphere. The magnetic susceptibility (χ) of the pristine **Cu-1** membrane was estimated to be $7.4 \times 10^{-4}\text{ emu mol}^{-1}$ at 300 K, which is consistent with the value of bulk **Cu-1**.^[16] Figure 4a depicts the χ values at 300 K under 10 kOe as a function of time, beginning when the water was dropped onto the membranes; the contributions from water ($-7.2 \times 10^{-7}\text{ emu g}^{-1}$) and core diamagnetism were not subtracted. The χ value in the initial state ($-1.6 \times 10^{-3}\text{ emu mol}^{-1}$ after ca. 1 min) steadily increased with time and eventually reached $-9.3 \times 10^{-4}\text{ emu mol}^{-1}$ after 1 h. The gradual increase in χ after 1 h is attributed to the evaporation of water (Figure S9 shows a linear increase up to 8 h). The magnitude of the χ increase ($7.7 \times 10^{-4}\text{ emu mol}^{-1}$) is in excellent agreement with the difference in χ at RT, i.e., $7.4 \times 10^{-4}\text{ emu mol}^{-1}$ for **Cu-1**^[16] and $1.4 \times 10^{-3}\text{ emu mol}^{-1}$ for **Cu-2**.^[17b] Apparently, the two-fold increase in net χ arises from the significant change in coordination structure upon the transformation of dimeric **Cu-1** into uniform-chain **Cu-2** while maintaining the 2D layered structure.

The kinetics of **Cu-1** to **Cu-2** were investigated via time-dependent in-plane magnetic susceptibility at different temperatures (280, 290, 300, and 310 K). As shown in Figure 5a, the increase in the content of **Cu-2** (α), which was estimated by normalizing the χ values using a linear interpolation after subtracting the water and core diamagnetism, becomes more rapid at higher temperature. We found that the $-\ln(1-\alpha)$ can be linearly related to time (t) in the \ln – \ln plot (Figure 5b), indicating the structural transformation within the framework of the Avrami–Erofe'ev model (eq 1)^[26] or its linear equivalent, the Sharp–Hancock equation (eq 2),^[26a,26b,27]

$$\alpha = 1 - e^{-(kt)^n} \quad (1)$$

$$\ln[-\ln(1-\alpha)] = n\ln(k) + n\ln(t) \quad (2)$$

where k is the kinetic constant of the transformation. According to the diffusion-controlled nuclei growth model, the n value (Avrami

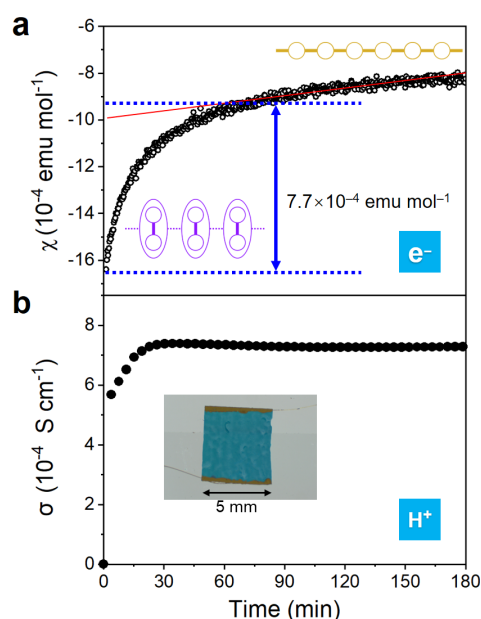


Figure 4. (a) In situ in-plane magnetic susceptibility (χ) of the membranes at 300 K under ambient helium atmosphere as a function of time, beginning when the water was dropped onto the membranes. The applied magnetic field is 10 kOe, and the contributions of water and core diamagnetism were not subtracted. The linear increase in χ after ca. 1 h probably arises from the gradual evaporation of water (red line; Figure S9). The inset shows the schematic electronic structures of **Cu-1** (purple) and **Cu-2** (yellow). The open circles and ellipsoids indicate Cu(II) ions with an $S = 1/2$ spin and Cu(II) dimer, respectively, whereas the thick-solid and thin-dotted lines indicate strong and weak magnetic interactions, respectively. (b) In situ in-plane proton conductivity (σ) as a function of time, where the initial time corresponds to the time at which water was dropped onto the membrane. Two gold wires were attached to the edge of both sides of the membrane with gold paste as the electrodes as shown in the inset.

exponent) is related to the growth mechanism and dimensions; $n = \beta + \lambda/2$ with nucleation factor β (0 for site saturation nucleation or zero nucleation mechanism and 1 for continuous nucleation with constant nucleation rate) and dimensional factor λ (1, 2, and 3 for 1D, 2D, and 3D, respectively).^[27,28] The low n values, which were estimated to be 0.600, 0.753, 0.798, and 0.727 at 280, 290, 300, and 310 K, respectively, based on the slope of Figure 5b, are indicative of the site saturation nucleation (i.e., all nucleation at $t = 0$) with $\beta \approx 0$.^[29] As a result, the λ values ranging from 1.2 to 1.6 are not inconsistent with the 2D diffusion-controlled mechanism ($\lambda \approx 2$) as expected from the 2D-to-2D structural transformation. Although a given n value does not necessarily allow different transformation mechanisms to be distinguished, it is apparent that the mechanism of the present transformation remains virtually unchanged over the temperature range measured. The activation energy (E_a) of the transformation was determined from the slope of the Arrhenius plot of $\ln(k)$ against T^{-1} (Figure 5c). The E_a value of 0.38 eV is much smaller than those of the formation of conventional CPs (> 1.3 eV in most cases),^[26a] which indicates that the present solid-state transformation is kinetically liable as manifested in the transformation proceeded even at RT. The potential energy of **Cu-2** relative to **Cu-1** was calculated to be -0.11 eV using the Perdew-Burke-Ernzerhof (PBE) functional and projector-augmented-wave pseudopotential on the reported crystallographic data (see the Supporting Information for details). Thus, it is apparent that the application of heat allows to overcome

an energy barrier with 0.38 eV to induce the thermodynamically stable **Cu-2**. The energy diagram constructed by the combination of experimental and theoretical approaches is displayed in Figure 5d.

Furthermore, we examined the time-dependent proton conductivity (Figure 4b), because one of the physical properties most affected by the coordination of water to copper ions in **Cu-2** is proton conduction owing to the possible proton hopping event between the Lewis-basic oxygen atoms.^[30] Crystallographic study has revealed that **Cu-2** involves the infinite hydrogen bonding network of coordinated water molecules along the c axis (i.e., in-plane direction; Figure S10a),^[17b] which is absent in **Cu-1**. The shortest O...O distance between the water molecules was estimated to be 3.01 Å, which is comparable to the sum of van der Waals radii (3.04 Å).^[31] Thus, the in-plane a.c. impedance spectra of the membrane were measured in situ during the **Cu-1**-to-**Cu-2** transformation. As displayed in the Figure 4b, the in plane proton conductivity significantly increases with time elapsed after water was dropped onto the membrane (Figure S11) from $\sigma = 3.0 \times 10^{-10}$ S cm $^{-1}$ in the initial state (**Cu-1** under dry condition) to $\sigma = 7.2 \times 10^{-4}$ S cm $^{-1}$ after 1 h (**Cu-2** under wet condition). The increase in σ is apparently associated with the structural transformation of **Cu-1** into **Cu-2**, which have different coordination topologies within the 2D sheet. It should be noted that the time when the σ value shows a rapid increase (< 20 min) is comparable to the half-time ($t_{1/2}$), which is defined as the time required for the α value to reach 50%, of 14.6 min at 300 K as shown in Figure 4b. In addition, the out-of-plane proton conductivity significantly increases with time (from $\sigma = 5.9 \times 10^{-10}$ S cm $^{-1}$ in the initial state to $\sigma = 1.6 \times 10^{-6}$ S cm $^{-1}$ after 1 h), although the σ value is two orders of magnitude lower than the in-plane value (Figure S12). The same reasoning as that given for the increased in-plane conduction should apply here, that is, the occurrence of an interlayer and cross-layer water network through

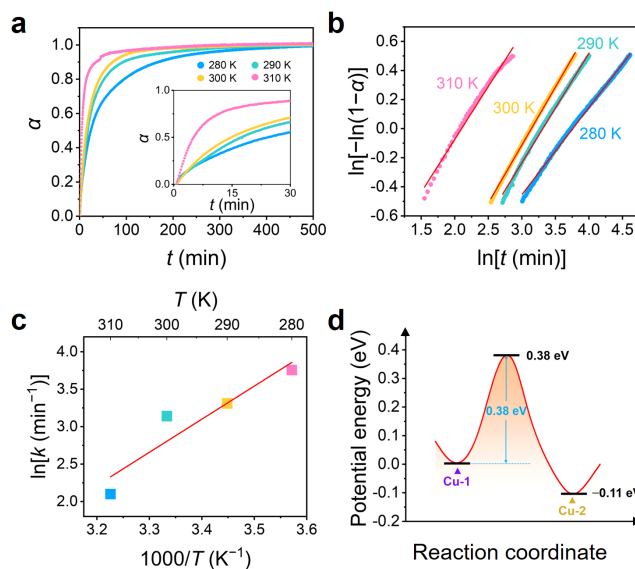


Figure 5. (a) Time dependence of the content of **Cu-2** (α) at 280 K (blue), 290 K (green), 300 K (orange), and 310 K (pink). Inset: Enlarged figure in the range of 0–30 min. (b) Avrami plots for the transformation of **Cu-1** to **Cu-2** at different temperatures. Red lines are the fit of the data to eq 2. (c) Arrhenius plot of the kinetic constants obtained from the Avrami plot, where the red line is the linear fit to the data. (d) Proposed energy profile of the transformation from **Cu-1** to **Cu-2**, where the energy is relative to that of **Cu-1**.

RESEARCH ARTICLE

O–H···O hydrogen bonds in **Cu-2** (Figure S10b). It should be stressed that vigorous stirring of the pulverized **Cu-2** membrane in water followed by thermal treatment in DMF can reversibly yield the starting **Cu-1** (Figure S13). Accordingly, the modification of the copper coordination environment with the release of dimerized copper units leads to the increased χ , whereas the exchange of coordinated solvents followed by the formation of the hydrogen bonding network results in the increased σ . The observed electronic and protonic behavior must be a reflection of the significant structural change in the 2D sheet while maintaining the layered structure, which can be readily induced only by immersing the membrane in water at RT.

Conclusion

Acknowledgements

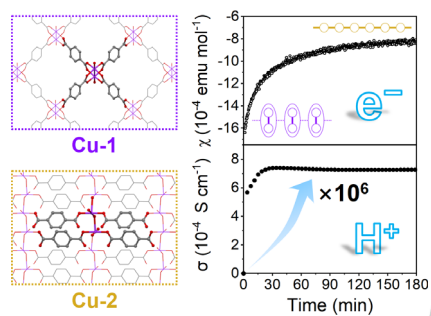
The authors are grateful to Dr. Akihiro Otsuka (Kyoto University) and Dr. Shiho Moriguchi (Shimadzu Techno-Research Incorporated) for their technical support. This work was supported by the ACCEL program (JPMJAC1501) of the Japan Science and Technology Agency (JST), JSPS KAKENHI (Grant No. 20H02708 and 20H05623), and the Research Budget from Nihon University School of Medicine. Part of the calculations was performed on CCMS supercomputer, Kyoto University.

Keywords: Coordination polymer • 2D-to-2D transformation • Magnetism • Proton conductivity

- [1] K. S. Novoselov, A. K. Geim, S. V. Morozov, D. Jiang, Y. Zhang, S. V. Dubonos, I. V. Grigorieva, A. A. Firsov, *Science* **2004**, *306*, 666–669.
- [2] a) A. K. Geim, I. V. Grigorieva, *Nature* **2013**, *499*, 419–425; b) C. Tan, X. Cao, X.-J. Wu, Q. He, J. Yang, X. Zhang, J. Chen, W. Zhao, S. Han, G.-H. Nam, M. Sindoro, H. Zhang, *Chem. Rev.* **2017**, *117*, 6225–6331; c) G. Chakraborty, I.-H. Park, R. Medishetty, J. J. Vittal, *Chem. Rev.* **2021**, *121*, 3751–3891.
- [3] a) S. Latil, L. Henrard, *Phys. Rev. Lett.* **2006**, *97*, 036803; b) B. Partoens, F. M. Peeters, *Phys. Rev. B* **2006**, *74*, 075404.
- [4] a) A. Splendiani, L. Sun, Y. Zhang, T. Li, J. Kim, C.-Y. Chim, G. Galli, F. Wang, *Nano Lett.* **2010**, *10*, 1271–1275; b) A. Kuc, N. Zibouche, T. Heine, *Phys. Rev. B* **2011**, *83*, 245213.
- [5] a) M. Naguib, V. N. Mochalin, M. W. Barsoum, Y. Gogotsi, *Adv. Mater.* **2014**, *26*, 992–1005; b) L. Jiang, D. Zhou, J. Yang, S. Zhou, H. Wang, X. Yuan, J. Liang, X. Li, Y. Chen, H. Li, *J. Mater. Chem. A* **2022**, *10*, 13651–13672.
- [6] a) M. Yankowitz, S. Chen, H. Polshyn, Y. Zhang, K. Watanabe, T. Taniguchi, D. Graf, A. F. Young, Dean, C. R. *Science* **2019**, *363*, 1059–1064; b) L. Balents, C. R. Dean, D. K. Efetov, A. F. Young, *Nat. Phys.* **2020**, *16*, 725–733.
- [7] a) H.-L. Jiang, T. A. Makal, H.-C. Zhou, *Coord. Chem. Rev.* **2013**, *257*, 2232–2249; b) S. R. Batten, R. Robson, *Angew. Chem. Int. Ed.* **1998**, *37*, 1460–1494.
- [8] T. Kuila, S. Bose, A. K. Mishra, P. Khanra, N. H. Kim, J. H. Lee, *Prog. Mater. Sci.* **2012**, *57*, 1061–1105.
- [9] a) X. Li, J. Shan, W. Zhang, S. Su, L. Yuwen, L. Wang, *Small* **2017**, *13*, 1602660; b) A. Stergiou, N. Tagmatarchis, *Chem. Eur. J.* **2018**, *24*, 18246–18257.
- [10] a) H. Yu, Y. Wang, Y. Jing, J. Ma, C.-F. Du, Q. Yan, *Small* **2019**, *15*, 1901503. b) H. Huang, R. Jiang, Y. Feng, H. Ouyang, N. Zhou, X. Zhang, Y. Wei, *Nanoscale* **2020**, *12*, 1325–1338.
- [11] a) S. Kitagawa, M. Kondo, *Bull. Chem. Soc. Jpn.* **1998**, *71*, 1739–1753; b) W. Lu, Z. Wei, Z. Y. Gu, T. F. Liu, J. Park, J. Park, J. Tian, M. Zhang, Q. Zhang, T. Gentle, M. Bosch, H. C. Zhou, *Chem. Soc. Rev.* **2014**, *43*, 5561–5593; c) S.-Y. Ke, C.-C. Wang, *CrystEngComm* **2015**, *17*, 8776–8785; d) A. Schoedel, M. Li, D. Li, M. O’Keeffe, O. M. Yaghi, *Chem. Rev.* **2016**, *116*, 12466–12535; e) R. E. Morris, L. Brammer, *Chem. Soc. Rev.* **2017**, *46*, 5444–5462; f) L. S. Xie, G. Skorupskii, M. Dincă, *Chem. Rev.* **2020**, *120*, 8536–8580; g) N. Behera, J. Duan, W. Jin, S. Kitagawa, *EnergyChem* **2021**, *3*, 100067.
- [12] G. K. Kole, J. J. Vittal, *Chem. Rev.* **2013**, *42*, 1755–1775.
- [13] H. Sato, R. Matsuda, M. H. Mir, S. Kitagawa, *Chem. Commun.* **2012**, *48*, 7919–7921.
- [14] a) J. Albalad, J. Arriñez-Soriano, J. Vidal-Gancedo, V. Lloveras, J. Juanhuix, I. Imaz, N. Aliaga-Alcalde, D. MasPOCH, *Chem. Commun.* **2016**, *52*, 13397–13400; b) J.-R. Zhang, J.-J. Lee, C.-H. Su, M.-J. Tsai, C.-Y. Li, J.-Y. Wu, *Dalton Trans.* **2020**, *49*, 14201–14215; c) Y. Wu, M. I. Breeze, D. O’Hare, R. I. Walton, *Microporous Mesoporous Mater.* **2017**, *254*, 178–183; d) X. Zhou, J. Dong, Y. Zhu, L. Liu, Y. Jiao, H. Li, Y. Han, K. Davey, Q. Xu, Y. Zheng, S.-Z. Qiao, *J. Am. Chem. Soc.* **2021**, *143*, 6681–6690.
- [15] a) C. G. Carson, K. Hardcastle, J. Schwartz, X. Liu, C. Hoffmann, R. A. Gerhardt, R. Tannenbaum, *Eur. J. Inorg. Chem.* **2009**, *2009*, 2338–2343; b) C. G. Carson, G. Brunello, S. G. Lee, S. S. Jang, R. A. Gerhardt, R. Tannenbaum, *Eur. J. Inorg. Chem.* **2014**, *2014*, 2140–2145.
- [16] Y. Jing, Y. Yoshida, P. Huang, H. Kitagawa, *Angew. Chem. Int. Ed.* **2022**, *61*, e202117417.
- [17] a) S. Cueto, V. Gramlich, W. Petter, F. S. Rys, P. Rys, *Acta Crystallogr.* **1991**, *C47*, 75–78; b) L. Deakin, A. M. Arif, J. S. Miller, *Inorg. Chem.* **1999**, *38*, 5072–5077.
- [18] S. Zhao, Y. Wang, J. Dong, C. He, H. Yin, P. An, K. Zhao, X. Zhang, C. Gao, L. Zhang, J. Lv, J. Wang, J. Zhang, A. M. Khattak, N. A. Khan, Z. Wei, J. Zhang, S. Liu, H. Zhao, Z. Tang, *Nat. Energy* **2016**, *1*, 16184.
- [19] a) T. Rodenas, I. Luz, G. Prieto, B. Seoane, H. Miro, A. Corma, F. Kapteijn, F. X. Llabrés i Xamena, J. Gascon, *Nat. Mater.* **2015**, *14*, 48–55; b) G. Zhan, L. Fan, F. Zhao, Z. Huang, B. Chen, X. Yang, S.-f. Zhou, *Adv. Funct. Mater.* **2019**, *29*, 1806720.
- [20] K. Tan, N. Nijem, P. Canepa, Q. Gong, J. Li, T. Thonhauser, Y. J. Chabal, *Chem. Mater.* **2012**, *24*, 3153–3167.
- [21] M. Nara, H. Torii, M. Tasumi, *J. Phys. Chem.* **1996**, *100*, 19812–19817.
- [22] a) V. Paredes-García, R. C. Santana, R. Madrid, A. Vega, E. Spodine, D. Venegas-Yazigi, *Inorg. Chem.* **2013**, *52*, 8369–8377; b) T. D. Smith, J. R. Pilbrow, *Coord. Chem. Rev.* **1974**, *13*, 173–278.
- [23] R. Maurice, K. Sivalingam, D. Ganyushin, N. Guihery, C. de Graaf, F. Neese, *Inorg. Chem.* **2011**, *50*, 6229–6236.
- [24] A. Ozarowski, *Inorg. Chem.* **2008**, *47*, 9760–9762.
- [25] A. Abragam, B. Bleaney, *Electron Paramagnetic Resonance of Transition Ions*, Clarendon Press: Oxford, **1970**.
- [26] a) M. J. Van Vleet, T. Weng, X. Li, J. R. Schmidt, *Chem. Rev.* **2018**, *118*, 3681–3721; b) A. Khawam, D. R. Flanagan, *J. Pharm. Sci.* **2006**, *95*,

- 472–498; c) M. Avrami, *J. Chem. Phys.* **1940**, *8*, 212–224; d) B. V. Erofe'ev, *Dokl. Akad. Nauk SSSR* **1946**, *52*, 511–514.
- [27] J. D. Hancock, J. H. Sharp, *J. Am. Ceram. Soc.* **1972**, *55*, 74–77.
- [28] a) S. F. Hulbert, *J. Br. Ceram. Soc.* **1969**, *6*, 11–20; b) F. Liu, S. J. Song, J. F. Xu, J. Wang, *Acta Mater.* **2008**, *56*, 6003–6012.
- [29] S. S. Farvid, P. V. Radovanovic, *J. Am. Chem. Soc.* **2012**, *134*, 7015–7024.
- [30] a) P. Colomban, Proton Conductors: Solids, *Membranes and Gels-Materials and Devices* (Ed.: H. Baxter), Cambridge University Press, **1992**. b) K. D. Kreuer, *Chem. Mater.* **1996**, *8*, 610–641; c) D. W. Lim, H. Kitagawa, *Chem. Rev.* **2020**, *120*, 8416–8467.
- [31] A. Bondi, *J. Phys. Chem.* **1964**, *68*, 441–451.

Entry for the Table of Contents



A 2D-to-2D structural transformation with a significant change in the coordination environment within the 2D layer was achieved in a copper-based coordination polymer in water at room temperature. The transformation led to large changes in the physical properties of the coordination polymers, such as proton conductivity and magnetism.